Spatial-temporal recurrent reinforcement learning for autonomous ships

Martin Waltz^{a,*}, Ostap Okhrin^a

^aTechnische Universität Dresden, Chair of Econometrics and Statistics, esp. in the Transport Sector, Dresden, 01062, Germany

Abstract

The paper proposes a spatial-temporal recurrent neural network architecture for Deep Q-Networks to steer an autonomous ship. The network design allows handling an arbitrary number of surrounding target ships while offering robustness to partial observability. Further, a state-of-the-art collision risk metric is proposed to enable an easier assessment of different situations by the agent. The COLREG rules of maritime traffic are explicitly considered in the design of the reward function. The final policy is validated on a custom set of newly created single-ship encounters called "Around the Clock" problems and the commonly chosen Imazu (1987) problems, which include 18 multi-ship scenarios. Additionally, the framework shows robustness when deployed simultaneously in multi-agent scenarios. The proposed network architecture is compatible with other deep reinforcement learning algorithms, including actor-critic frameworks.

Keywords: deep reinforcement learning, recurrency, autonomous surface vehicle, COLREG

1. Introduction

Recently, Silver et al. (2021) hypothesized that any form of intelligence and its associated abilities can be considered as a form of maximizing a reward signal. Thus, the reward-based field of Reinforcement Learning (RL, Sutton and Barto 2018) might offer unprecedented potential to master var-

Email address: martin.waltz@tu-dresden.de (Martin Waltz)

^{*}Corresponding author

ious real-world control tasks. Combined with neural networks as function approximators, Deep Reinforcement Learning (DRL) approaches have shown remarkable performances in complex strategy games (Vinyals et al., 2019), advanced racing simulations (Wurman et al., 2022), or even in the autonomous navigation of stratospheric balloons over the Pacific Ocean (Bellemare et al., 2020). Especially the safety-critical traffic domain can benefit from reliable, autonomously controlled ships. Human error is still the primary cause of accidents. In maritime traffic, the Annual Overview of Marine Casualties and Incidents 2021 from the European Maritime Safety Agency (European Maritime Safety Agency, 2021) reports that from 2014-20 over 53% of the accident events are caused by human actions. The perspective of achieving lower accident rates in maritime operations while increasing energy and time efficiency created massive academic interest in the design of autonomous surface vehicles (ASV) in recent years (Cheng and Zhang, 2018; Zhao and Roh, 2019; Xu et al., 2022a; Hart et al., 2022).

Vagale et al. (2021b) define ASVs as vessels that can make decisions and operate independently without requiring human guidance, navigation, and control. An elementary characteristic of such systems is the ability to reliably plan and follow a path towards a specified end position while avoiding collisions with other ships. Next to DRL, there are various deterministic and heuristic methodological approaches to designing ASVs. Popular examples include the A* path-planning algorithm (Hart et al., 1968; Loe, 2008), and its modifications (Singh et al., 2018; Liu et al., 2019), velocity obstacles (Fiorini and Shiller, 1998; Huang et al., 2018, 2019), the artificial potential field method (Khatib, 1985; Wu et al., 2017), or genetic algorithms (Kramer, 2017; Li et al., 2019). We refer the reader to Vagale et al. (2021a) and Zhai et al. (2022) for discussions and comprehensive literature reviews. Crucially, next to the inherent limitations of these approaches, the Convention on the International Regulations for Preventing Collisions at Sea (COLREG) are generally not considered. The convention is a set of rules from the International Maritime Organization (1972), which should improve maritime traffic safety by specifying how seafarers should behave in certain encounter situations. Each vessel on high seas or in connected navigable waters must follow the COLREG rules. Consequently, any practical ASV algorithm should account for them. The current industry-proven low-level controllers, or autopilots, cannot cope with the complex requirements of high-level path planning and COLREG-compliant collision avoidance, as stated by Heiberg et al. (2022).

There has been a series of proposals to implement DRL on ASVs. Cheng

and Zhang (2018) proposed a concise DRL obstacle avoidance algorithm based on the Deep Q-Networks (DQN, Mnih et al. 2015) to maneuver through static obstacles. Xu et al. (2022a) detailed a modification of the Deep Deterministic Policy Gradient (DDPG, Lillicrap et al. 2015) algorithm to construct an autonomous collision avoidance algorithm under consideration of COL-REGs. The DDPG also builds the methodological basis for the ASV obstacle avoidance in Zhou et al. (2022), although this study lacks explicit consideration of the traffic rules. Sawada et al. (2021) implement an automatic collision avoidance based on the obstacle zone target to predict whether vessels will collide in the future. Further contributions include Xu et al. (2020), Meyer et al. (2020), Chun et al. (2021), and Xu et al. (2022b).

All the studies above have in common that the ownship (OS), which is the ASV controlled by the RL agent, must aggregate information of surrounding target ships (TS) to assess the collision risk (CR) of a situation and ultimately select an action. The TS information can be provided by the Automatic Identification System (AIS), mandatory equipment for vessels of specific sizes. The AIS can be considered a feature vector per TS and contains information such as position, course, heading, and speed. On this basis, two critical challenges arise.

The first challenge is, how do we adequately process these vectors when the numbers of target ships vary? The input size of a fully-connected neural network is fixed. To tackle this issue, several simplifying assumptions and practices have been used. Chun et al. (2021) and Xu et al. (2022a) consider only the TS with highest collision risk, while neglecting all other information. Xu et al. (2020) fix a certain number of target ships and train an extra agent for each configuration. Zhao and Roh (2019) pre-cluster the input according to four COLREG-directions, see Section 2.2. Finally, some studies move to entirely different observation formats like LiDAR beams (Li et al., 2021; Zhou et al., 2022; Meyer et al., 2020) or visual grid input (Woo and Kim, 2020; Sawada et al., 2021). The second challenge is, how do we create a robust framework under partial observability, considering that the received data may offer delay, noise, or weather-based disturbances (Almalioglu et al., 2022)? Acknowledging that AIS data might not be high-frequent enough to generate sufficient situational awareness in crowded areas (Heiberg et al., 2022), the algorithm should process information of several time steps instead of solely relying on the current observation.

In this paper, we leverage the potential of DRL by designing a simulationbased ASV agent that tackles both challenges. Our contributions to the

literature are as follows:

- A spatial-temporal recurrent neural network architecture for the DQN is proposed. The approach extends prior work of Everett et al. (2018, 2021) from the robotic domain and enables to process information in multi-ship encounter situations with a variable number of target ships. Moreover, due to the integration of the temporal recurrent component, we achieve robustness against partial observability.
- A novel collision risk metric based on the concept of the closest point of approach (CPA, Lenart 1983) and the ship domain (Goodwin, 1975) is designed. Through the neural architecture and the CR metric, we avoid the hierarchical decomposition of the agent into different subcontrollers (see Zhai et al. 2022) and realize a robust, holistic solution.
- A suitable training environment with a COLREG-dependent spawning routine of target ships is designed, in which the agent controls only the rudder angle of the vessel. Additionally, we create the *Around the Clock* problems as a comprehensive test-bed of single-ship encounters.
- Our agent is thoroughly validated in multi-encounter scenarios using the *Imazu problems* (Sawada et al., 2021) and two multi-agent situations called the *Star problems*, inspired by Zhao and Roh (2019). In all cases, the agent successfully reaches a specified destination, safely avoids collisions with other vessels, obeys maritime traffic rules, and performs realistic steering actions.

This paper is structured as follows: Section 2 introduces the modeling of maritime traffic, including the environmental dynamics model, details on the COLREGs, and the new CR metric. Section 3 presents the RL methodology, outlines the proposed neural network architecture, and describes the state, action, and reward configuration. Section 4 discusses our simulation environment used for training, while the validation scenarios are shown in Section 5. Section 6 concludes. We make the source code to this paper publicly available at https://github.com/MarWaltz/TUD_RL to enable full reproducibility.

2. Modeling of maritime traffic

2.1. Environmental dynamics

We consider the Maneuvering Modeling Group (MMG) model of Yasukawa and Yoshimura (2015) to describe the dynamics of the full-scale KVLCC2 (Stern et al., 2011) tanker. Several related works (Cheng and Zhang, 2018; Heiberg et al., 2022; Du et al., 2022) instead rely on the miniature model ship CyberShip II with the hydrodynamic parameters identified by Skjetne et al. (2004). However, we have chosen the KVLCC2 since it has a length between perpendiculars of $L_{pp} = 320 \,\mathrm{m}$, allowing for a more realistic setup on the ocean, and the corresponding dynamics model is identified and extensively tested in Yasukawa and Yoshimura (2015). Our simulation relies on the following assumptions, which are frequently imposed when modeling maritime traffic (Meyer et al., 2020; Heiberg et al., 2022):

Assumption 1: Calm sea. There are no external disturbances in form of wind, waves, or currents.

Assumption 2: Motion restriction. The vessel is located on a horizontal plane with no heave, pitch, and rolling motion.

Consequently, the model consists of 3 degrees of freedom in which the navigational state of the vessel is described by $\eta = [x_n, y_n, \psi]^{\top}$. The elements x_n and y_n are north and east coordinates relative to a coordinate origin o_n in the North-East-Down system $\{n\}$, where ψ is the vessel's heading and defined as the angle between the x_n -axis and the x_b -axis of the body-fixed reference frame $\{b\}$, which is centered at the midship position. In $\{b\}$, x_b corresponds to the longitudinal axis, while y_b is the transversal (starboard) axis. The velocity of the vessel is described by $\nu = [u, v, \tilde{r}]^{\top}$, where u and v are the components in x_b - and y_b -direction, respectively, and \tilde{r} is the yaw rate. Furthermore, we define the drift angle $\beta = \arctan(v/u)$, the total speed $U = \sqrt{u^2 + v^2}$, and the course angle $\chi = \psi + \beta$ (Fossen, 2021). Figure 1 illustrates the coordinate systems. The following set of equations connects $\{n\}$ and $\{b\}$ via rotation:

$$\dot{x}_n = u \cos \psi - v \sin \psi,
\dot{y}_n = u \sin \psi + v \cos \psi,
\dot{\psi} = \tilde{r},$$
(1)

where \dot{w} denotes the (later component-wise) first order derivative of w. The equations of motions governing the dynamics of the vessel are:

$$(m + m_{x_b})\dot{u} - (m + m_{y_b})v\tilde{r} - x_G m\tilde{r}^2 = X = X_H + X_R + X_P,$$

$$(m + m_{y_b})\dot{v} + (m + m_{x_b})u\tilde{r} + x_G m\dot{\tilde{r}} = Y = Y_H + Y_R,$$

$$(I_{zG} + x_G^2 m + J_z)\dot{\tilde{r}} + x_G m(\dot{v} + u\tilde{r}) = N_m = N_H + N_R,$$
(2)

where m is the ship's mass, m_{x_b}, m_{y_b} are the added masses in x_b and y_b direction, respectively, x_G is the longitudinal coordinate in $\{b\}$ of the center of gravity (COG) of ship, I_{zG} is the moment of inertia of the ship around the COG, and J_z is the added moment of inertia. Further, X is the surge force, Y is the lateral force, and N_m is the yaw moment around midship. These forces consist of their respective hull (H), rudder (R), and propeller (P) components. Yasukawa and Yoshimura (2015) contains the detailed expressions for each force alongside parameters for the full-scale KVLCC2 tanker, and we refer the reader interested in the fine details to this paper. Crucially, by adjusting the tanker's rudder angle δ , we control the related rudder forces X_R , Y_R , and N_R and can realize steering commands.

We use a subscript t to refer to a particular quantity at time t, e.g., η_t and ν_t for the navigation and velocity vector, respectively. We discretize the dynamics using a step-size of 3 seconds, thus η_{t+1} corresponds to being 3 seconds in real-time after η_t . To obtain η_{t+1} and ν_{t+1} , we solve the systems of equations (1) and (2) for the derivatives $\dot{\eta}_t$ and $\dot{\nu}_t$, and use the ballistic method of Treiber and Kanagaraj (2015). The latter consists of an Euler update for the speeds and a trapezoidal update for the positions.

2.2. International Regulations for Preventing Collisions at Sea

2.2.1. Overview

Compliance with the COLREG rules of the International Maritime Organization (1972) is mandatory for vessels operating on high seas. However, the 41 rules lack specific, measurable quantities to determine whether a particular behavior was COLREG-compliant or not. Notably, in the 1970s, when the rules were published, there were no autonomous vessel systems, and the regulation was tailored to human seafarers and decision-makers. As pointed out by Heiberg et al. (2022), modern optimization approaches do not necessarily produce COLREG-compliant actions. For example, collision avoidance actions must be substantial and visible to make the agent's intentions transparent to other traffic participants. However, such behavior does

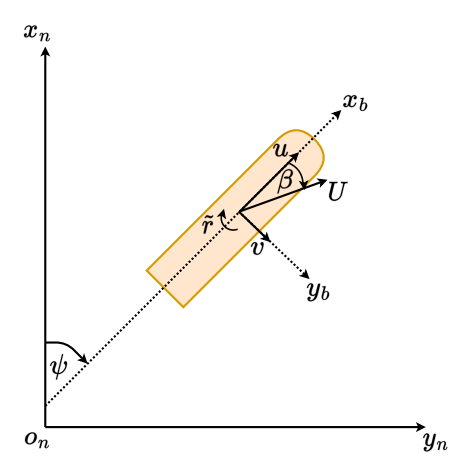


Figure 1: Visualization of the coordinates systems $\{n\}$ and $\{b\}$ similar to Yasukawa and Yoshimura (2015).

mostly not equate to fuel or time efficiency. The combination of autonomous and human-controlled vessels and potential changes to the regulatory rule set constitute an active area of research (Zhou et al., 2020; Miyoshi et al., 2022).

For the reader's convenience, Appendix A contains concrete passages of the rules that are especially relevant for maritime traffic modeling. To briefly summarize the most important COLREGs, each vessel should proceed at a safe speed to effectively avoid collisions, determine if the risk of collision exists, and take substantial collision avoidance actions to pass other vessels at a safe distance. Moreover, the COLREGs categorize vessels into giveway and stand-on, depending on their role in one of four possible encounter situations, see Figure 2. Generally, give-way vessels are required to keep out of the other vessel's way, while stand-on vessels should keep their course and speed. For example, both vessels are classified as give-way in a Head-On scenario (Figure 2, Panel 1) and should change their course to starboard.

Similar to Woo and Kim (2020) and Xu et al. (2022b), we will assume that the target ships move linear and deterministic in our simulation. Therefore, our work focuses on cases where the OS is the give-way ship and is responsible for actively avoiding collisions. Section 2.2.2 discusses the criteria for the presence of each encounter scenario.

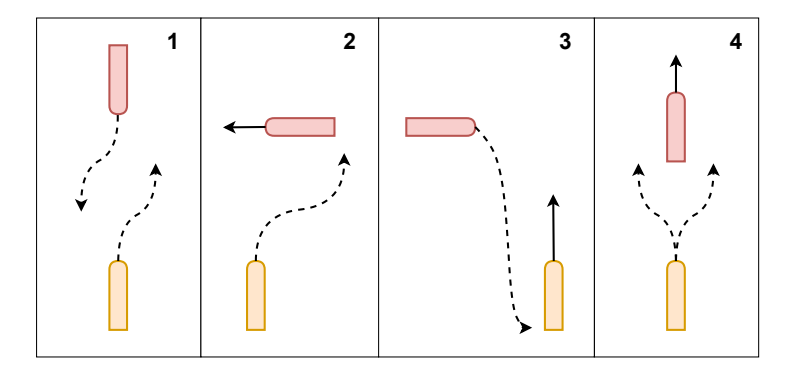


Figure 2: Visualization of the COLREG encounter situation based on Vagale et al. (2021b). The OS is the yellow one and the TS is red. There are four scenarios: (1) Head-On, (2) Starboard crossing, (3) Port crossing, and (4) Overtaking. The give-way vessel is depicted with a dashed line, while the stand-on vessel has a solid line.

2.2.2. Scenario classification

Whether a scenario at sea is classified as one of the four encounter situations depends on the two vessels' angular and positional constellation, measured in two quantities, see Figure 3. First, the heading intersection angle $C_T = [\psi_{TS} - \psi_{OS}]_0^{2\pi}$, where ψ_{TS} and ψ_{OS} are the headings of the TS and the OS, respectively, with the clipping operation to $[a, a + 2\pi)$ for $a \in \{-\pi, 0\}$, defined as $[\cdot]_a^{a+2\pi}$:

$$[\theta]_a^{a+2\pi} = \begin{cases} \theta - \left\lfloor \frac{\theta-a}{2\pi} \right\rfloor \cdot 2\pi & \text{if } \theta \ge 0, \\ \theta + \left(\left\lfloor \frac{-\theta-a}{2\pi} \right\rfloor + 1 \right) \cdot 2\pi & \text{if } \theta < 0, \end{cases}$$

where the floor operator, which returns the largest integer smaller than the argument, is denoted by $|\cdot|$ (Benjamin, 2017).

Second, α_{OS}^{TS} , the relative bearing from the OS to the TS, which is computed as the difference between the absolute bearing, β_{OS}^{TS} , and the OS's heading: $\alpha_{OS}^{TS} = \left[\beta_{OS}^{TS} - \psi_{OS}\right]_0^{2\pi}$. Vice versa, α_{TS}^{OS} and β_{TS}^{OS} are the quantities from the perspective of the TS toward the OS. On the basis of the heading intersection angle and the relative bearing, the scenarios can be classified according to Table 1, and sketched in Figure 2. Note that the rules should always be seen in context to the present situation at sea, and seafarers consider softly defined practices referred to as good seamanship.

Moreover, the definitions above focus solely on situations with two vessels. In practice, multi-ship situations are possible, especially in highly congested

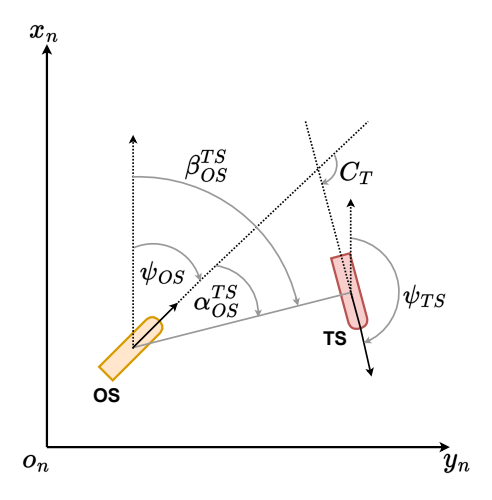


Figure 3: Visualization of the heading intersection angle C_T , the relative bearing α_{OS}^{TS} , and the absolute bearing β_{OS}^{TS} .

sea areas. A reliable control system needs to effectively process information of all relevant target ships to find a safe path in those cases, despite the insufficiently defined rule set (Kang et al., 2021).

2.3. Collision risk assessment

2.3.1. Ship domain and CPA

Assessing the collision risk with other vessels is required by the COLREGs and constitutes a fundamental part of an ASV. The methodological repertoire of the literature is diverse and has recently been reviewed by Ozturk and Cicek (2019) and Huang et al. (2020). Two crucial approaches are the definition of ship domains (Goodwin, 1975; Śmierzchalski, 2005; Szlapczynski and Szlapczynska, 2017) and the concept of closest point of approach (Mou et al., 2010; Zhao and Roh, 2019). The ship domain is a safe area around the vessel, which should not be entered by other ships. Several geometric representations of ship domains have been considered, and they are primarily asymmetric with larger space on the starboard side to enable COLREG-compliant collision avoidance. While there are several possibilities for defining a collision based on a ship domain (Heiberg et al., 2022), in this study, we define the TS's midship position being at or inside the OS's ship domain as a collision event. While non-violation of the ship domain equates to reliable collision avoidance, the approach lacks a quantitative CR metric

Situation	σ	Requirements	Action from OS		
Head-On	1	$\alpha_{OS}^{TS} \in \{ [0^{\circ}, 5^{\circ}] \cup [355^{\circ}, 360^{\circ}) \}$ $C_T \in [175^{\circ}, 185^{\circ}]$	Alter course to starboard, pass TS on its portside		
Starboard crossing	2	$\alpha_{OS}^{TS} \in [5^{\circ}, 112.5^{\circ}]$ $C_T \in [185^{\circ}, 292.5^{\circ}]$	Alter course to starboard, avoid crossing ahead of TS		
Port crossing	3	$\alpha_{OS}^{TS} \in [247.5^{\circ}, 355^{\circ}]$ $C_T \in [67.5^{\circ}, 175^{\circ}]$	Keep course, TS is give-way vessel		
Overtaking	4	$\alpha_{TS}^{OS} \in [112.5^{\circ}, 247.5^{\circ}]$ $C_T \in \{[0^{\circ}, 67.5^{\circ}] \cup [292.5^{\circ}, 360^{\circ})\}$ $U_{OS,R} > U_{TS}$	Overtake at any side, keep out of TS's way		

Table 1: Classification of COLREG encounter situations between two vessels following Xu et al. (2020). We define the variable σ to refer to a particular scenario. If there are no requirements fulfilled, we set $\sigma=0$. Overtaking imposes next to the C_T and α_{OS}^{TS} a third constraint, namely that the relative speed of the OS in the direction of the TS's course, $U_{OS,R}$, is larger than the TS's total speed U_{TS} .

since violation or non-violation of the domain is a binary variable (Ha et al., 2021).

Filling this gap, the CPA concept describes the closest point two vessels will encounter under the assumption that both keep their course and speed. Two key quantities are the time until reaching the CPA, called TCPA, and the distance between the two vessels when being at the CPA, called DCPA (Lenart, 1983):

$$TCPA = -\frac{(x_{n,TS} - x_{n,OS}) \cdot v_{r,x_n} + (y_{n,TS} - y_{n,OS}) \cdot v_{r,y_n}}{v_{r,x_n}^2 + v_{r,y_n}^2},$$

$$\Delta x_{n,TCPA} = (x_{n,OS} + TCPA \cdot v_{x_{n,OS}}) - (x_{n,TS} + TCPA \cdot v_{x_{n,TS}}),$$

$$\Delta y_{n,TCPA} = (y_{n,OS} + TCPA \cdot v_{y_{n,OS}}) - (y_{n,TS} + TCPA \cdot v_{y_{n,TS}}),$$

$$DCPA = \sqrt{(\Delta x_{n,TCPA})^2 + (\Delta y_{n,TCPA})^2},$$
(3)

where $x_{n,OS}$, $y_{n,OS}$, $v_{x_{n,OS}}$, $v_{y_{n,OS}}$ are the positions and speeds of the OS in $\{n\}$, respectively. The notation for the TS is analogue, and the relative speeds are $v_{r,x_n} = v_{x_{n,TS}} - v_{x_{n,OS}}$ and $v_{r,y_n} = v_{y_{n,TS}} - v_{y_{n,OS}}$. The drawback of the CPA-based metrics is their inability to reliably guarantee collision avoid-

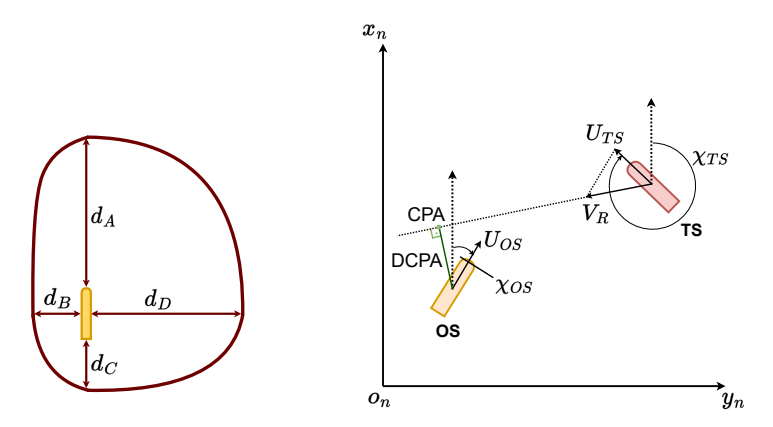


Figure 4: Visualization of the collision risk assessment methods used in this work. The left-hand side shows the asymmetric ship domain of Chun et al. (2021), which we construct as a combination of four ellipsis with $d_A = d_D = 3L_{pp}$ and $d_B = d_C = L_{pp}$. The right-hand side visualizes the concept of CPA and DCPA based on Heiberg et al. (2022). In this illustration, the heading equals the course angle for both vessels.

ance when analyzed in isolation (Ha et al., 2021), and the abstraction from present yaw moments and future non-linear behavior. Figure 4 illustrates the concepts.

2.3.2. Construction of a collision risk metric

The construction of a reliable collision risk metric is of central importance for an RL agent since it directly signals the criticality of an opposing ship. Based on the concepts from Section 2.3.1, we develop a novel CR metric, unifying the concepts CR_{CPA} and CR_{ED} to be defined later, as follows:

$$CR = \begin{cases} 1 & \text{if TS in ship domain of OS,} \\ \max(CR_{\text{CPA}}, CR_{\text{ED}}) & \text{otherwise.} \end{cases}$$
 (4)

The metric is in [0,1], where 0 suggests no risk of collision and 1 is a collision event. Through the maximum operator, we consider the more critical one of two components CR_{CPA} and CR_{ED} . The first one, CR_{CPA} , signals a large collision risk if TCPA (in absolute value) and DCPA are small since the OS then faces a potentially dangerous situation in the near future. The second component, CR_{ED} , assesses a small Euclidean distance between two ships as a high risk of collision. The necessity of introducing this second component is discussed in detail below.

Building on Mou et al. (2010), we define CR_{CPA} to behave exponentially in negative TCPA and DCPA:

$$CR_{\text{CPA}} = \exp\left\{c_1 \cdot \left[\text{DCPA}' + c_2^{\mathbf{1}\{\text{TCPA} \ge 0\}} \cdot c_3^{\mathbf{1}\{\text{TCPA} < 0\}} | \text{TCPA}|\right]\right\}, \quad (5)$$

where we set $c_1 = \log(0.1)/3704$, $c_2 = 1.5$, $c_3 = 20$ in our simulation. Note that 3704 meters equal 2 nautical miles (NM) and that the sign of c_1 is negative. The indicator function $\mathbf{1}\{x\}$ is 1 if x is true and 0 otherwise. Since we set $c_2 < c_3$, we weigh positive and negative TCPA differently and achieve a rapid decay in collision risk after the CPA has been passed while avoiding a jump in the metric by, e.g., setting the CR_{CPA} component zero. Furthermore, instead of directly using the DCPA from (3), we consider the distance of the TS to the OS's ship domain via the following modification:

$$DCPA' = f_{DCPA} \cdot \max \left[0, DCPA - D(\alpha_{OS,CPA}^{TS}) \right]. \tag{6}$$

The function $D(\cdot)$ returns the ship domain for a given encounter angle, which is non-constant since we consider an asymmetric shape; compare Figure 4. Further, we denote the relative bearing from the perspective of the OS towards the TS when being at the CPA, or equivalently, at TCPA = 0, with $\alpha_{\text{OS,CPA}}^{\text{TS}}$. Thus, we consider the safety area of the OS at the CPA. Furthermore, we want to explicitly avoid that the agent crosses at the bow of other ships, which is considered bad practice at sea. The factor f_{DCPA} is responsible for that:

$$f_{\text{DCPA}} = \begin{cases} c_4 - \exp(c_5 \cdot |[\alpha_{\text{TS;CPA}}^{\text{OS}}]_{-\pi}^{\pi}|) & \text{if TCPA} \ge 0 \text{ and } |[\alpha_{\text{TS;CPA}}^{\text{OS}}]_{-\pi}^{\pi}| \le \frac{\pi}{6}, \\ 1 & \text{otherwise,} \end{cases}$$

where $\alpha_{\mathrm{TS,CPA}}^{\mathrm{OS}}$ is the relative bearing from the perspective of the TS towards the OS at the CPA, and $c_4 = 1.2$, $c_5 = -\log(5)/\frac{\pi}{6}$ are constants. The factor penalizes the undesired crossing behavior by decreasing the sensed distance at the CPA and thus increasing the risk of collision. Figure 5 visualizes the behavior of the factor.

The component CR_{CPA} is a reasonable quantification of collision risk in the majority of scenarios. However, there are distinct disadvantages that made the inclusion of the component CR_{ED} based on the Euclidean distance between the ships, denoted $d_{\text{OS}}^{\text{TS}}$, necessary. Consider a scenario where two ships are close but have almost the same course. The CPA-based metrics

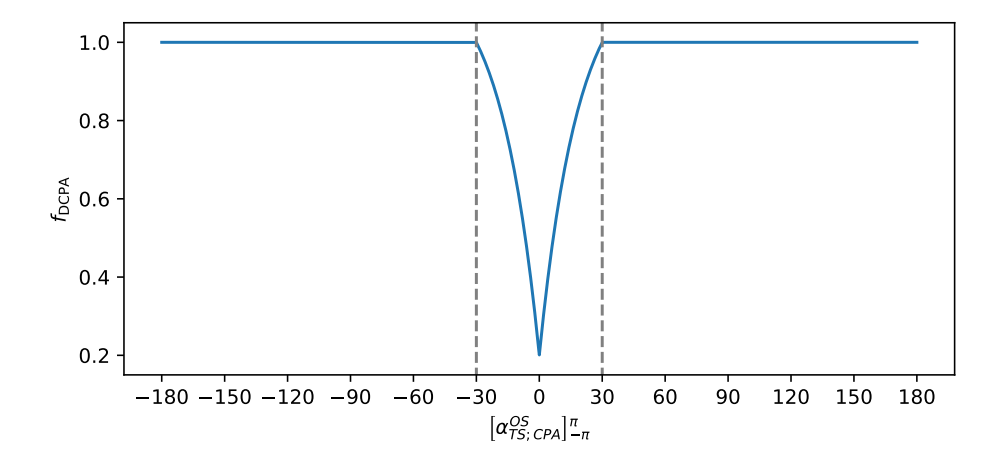


Figure 5: Specification of the factor f_{DCPA} for bow-crossing avoidance. The illustration shows the case $\text{TCPA} \geq 0$ and $[\alpha_{\text{TS;CPA}}^{\text{OS}}]_{-\pi}^{\pi}$ in degree.

signal that this situation is not risky since the CPA lies either a long time in the past or is far in the future. However, if a ship turns even slightly, the absolute value of the TCPA jumps to a much smaller value, and suddenly the situation is precarious. To prevent this drawback, we define the second component as follows:

$$CR_{\rm ED} = \exp\left\{c_6 \cdot \left[d_{\rm OS}^{\rm TS} - D(\alpha_{\rm OS}^{\rm TS})\right]\right\},\tag{7}$$

where $c_6 = -0.3 \cdot 3704 = -1111.2$ is a negative constant. The subtraction of the ship domain is motivated as in (6).

We emphasize that the functional relationships (4)-(7) build a robust collision risk metric for vessels of various classes. However, we set the constants c_1, \ldots, c_6 specifically for the KVLCC2 tanker, and these values should be adjusted for a vessel with different characteristics and manoeuvrability. Moreover, similar to how human seafarers have different interpretations of safe passing distances (Miyoshi et al., 2022), the ASV designer can calibrate c_1, \ldots, c_6 depending on how risk-avers the agent should be.

3. Reinforcement learning methodology

3.1. Background

Reinforcement learning is a methodological ensemble in which an agent learns based on trial-and-error in an environment (Sutton and Barto, 2018).

The common formalism of the problem is a Markov Decision Process (MDP, Puterman 1994) as the tuple (S, A, P, R, γ) . S is the state space, A is the discrete action space, $P: S \times A \times S \to [0, 1]$ is the state transition probability distribution, $R: S \times A \to \mathbb{R}$ is a bounded reward function, and $\gamma \in [0, 1)$ is the discount factor. At each step t, the agent receives state information $s_t \in S$, takes an action $a_t \in A$ according to a policy $\pi: S \times A \to [0, 1]$, gets a reward r_t generated by R, and transitions according to P to the next state $s_{t+1} \in S$. Transferred to our maritime application case, the state includes the positional and motion information of the ships, while the action is the change of the rudder angle from the OS.

The discounted sum of rewards during an episode is called return. Many frequently used RL algorithms define action-values: $Q^{\pi}(s, a) = E\left[\sum_{t=0}^{\infty} \gamma^{t} r_{t} | s_{0} = s, a_{0} = a\right]$. Thus, these so-called Q-values describe the expected return when executing action a in state s and following policy π afterward. The methodological basis of our work is the Q-Learning algorithm of Watkins and Dayan (1992). The objective of the algorithm is to attain the optimal action-values $Q^{*}(s, a)$ for all $s \in \mathcal{S}, a \in \mathcal{A}$, which yield an optimal policy: $\pi^{*}(s) = \arg \max_{a' \in \mathcal{A}} Q^{*}(s, a)$ for all $s \in \mathcal{S}, a \in \mathcal{A}$ if such an optimal policy exists; see Puterman (1994) for a deep discussion. The convergence conditions for Q-Learning are relatively mild (Tsitsiklis, 1994).

Storing a Q-value for each state-action pair is infeasible for continuous state spaces, which occur in our maritime environment. Mnih et al. (2015) proposed the DQN algorithm, an extension of Q-Learning where action-values are approximated by deep neural networks (DNN). More precisely, we consider the function $Q(s, a; \theta)$ for all $s \in \mathcal{S}, a \in \mathcal{A}$, where θ is the parameter set of the DNN. The optimization is performed by gradient descend:

$$\theta \leftarrow \theta + \tau \left[y - Q(s, a; \theta) \right] \nabla_{\theta} Q(s, a; \theta),$$

where $y = r + \gamma \max_{a' \in \mathcal{A}} Q(s', a'; \theta^-)$. The successor state after executing action a in state s is denoted s', τ is the learning rate, and θ^- is the parameter set of the target network, a time-delayed copy of θ . Moreover, the DQN uses experience replay to stabilize training.

3.2. Spatial-temporal recurrent architecture

In practice, observing the full state of a system is often not possible due to sensor limitations, noise, time-delays, and other factors. Acknowledging this circumstance, we formally consider a Partially Observable MDP (POMDP, Kaelbling et al. 1998), which extends the MDP-tuple (S, A, P, R, γ) of Section 3.1 by two components: the observation space \mathcal{O} , and the observation function $\mathcal{Z}: S \times A \times \mathcal{O} \to [0,1]$. At time t, instead of receiving the full state $s_t \in S$, the agent gets an observation $o_t \in \mathcal{O}$, which is generated by \mathcal{Z} . On an implementation level for the DQN, the action-value function receive as input an observation $o \in \mathcal{O}$ instead of the state $s \in S$.

Recently, Meng et al. (2021) proposed the LSTM-TD3 algorithm, an extension of the TD3 algorithm of Fujimoto et al. (2018) to deal with POMDPs. A memory extraction component based on a long short-term memory (LSTM, Hochreiter and Schmidhuber 1997) architecture processes several past observations, and combines the information with the observation of the current time step. Thus, the LSTM-TD3 incorporates a temporal recurrency, in which information of observation sequences over time are processed.

In our maritime application case, an observation $o_t = o_{OS,t} \cup o_{TS,t}$ consists of two components: $o_{OS,t}$, the information regarding the navigational status of the OS, and $o_{TS,t}$, the information of surrounding target ships. The observation $o_{TS,t}$ consists of features inspired by AIS data and will be detailed in Section 3.3. Importantly, the size of $o_{TS,t}$ is $N_t \cdot 6$, where N_t is the number of the target ships surrounding the OS at time t. Crucially, N_t can change over time, and the input size for a standard fully-connected neural network is not fixed. Building on Everett et al. (2018, 2021), we propose a more flexible approach by introducing a spatial recurrence that sequentially processes the target ships according to their estimated collision risk. Similar to the temporal LSTM looping over sequences of observations of different time steps, the introduced spatial LSTM loops over the sub-observations of different target ships at the same point of time.

In the proposed architecture, we implement both *temporal and spatial* recurrency components. Thus, we can deal with an arbitrary number of target ships while efficiently processing information over several time steps. Formally:

$$x_{t-l} = f_l(o_{OS,t-l}, o_{TS,t-l}; \theta_{f_l})$$
 for $l = 0, ..., h$,
 $Q(o_{(t-h):t}, a_i; \theta) = g(x_{t-h}, ..., x_{t-1}, x_t, a_i; \theta_g)$ for $i = 1, ..., M$,

where M is the cardinality of the action space and $o_{(t-h):t} = \bigcup_{l=0}^{h} o_{t-l}$. The number of considered past observations is h, and we fix h=2 throughout the paper since it already provides a very good performance. The functions f_l with parameters θ_{f_l} for $l=0,\ldots,h$ represent the spatial recurrency, and

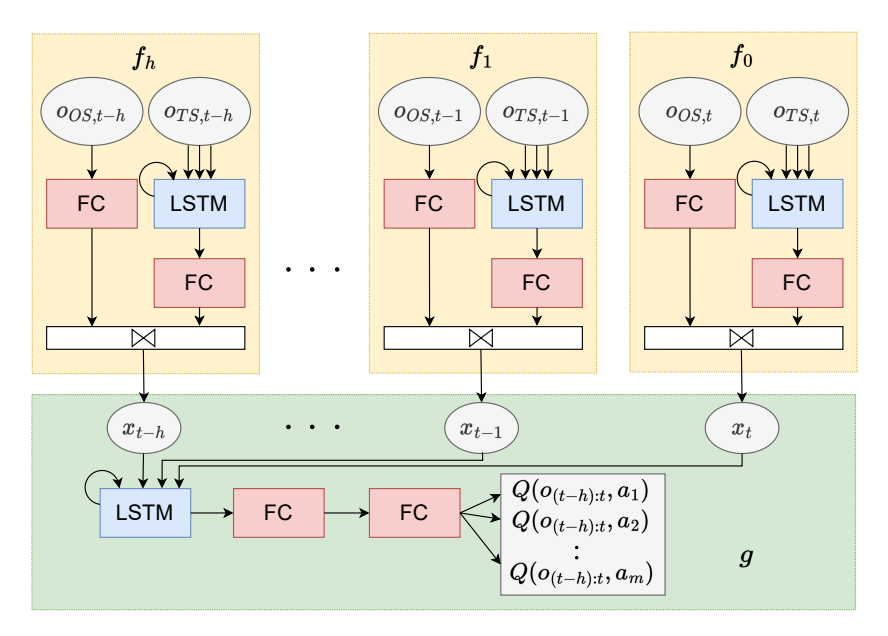


Figure 6: Spatial-temporal recurrent architecture. The concatenation symbol is \bowtie , and FC refers to a fully-connected layer with 64 output features as specified in deep learning frameworks like PyTorch (Paszke et al., 2019). Thus, strictly speaking, it is one weight matrix rather than a layer. We use ReLU activations after each FC block except for the last one, which applies the identity function to yield Q-value estimates in \mathbb{R}^M . The number of hidden units in the LSTM blocks is 64.

the function g, parametrized by θ_g , corresponds to the temporal recurrency. The complete parameter set is $\theta = \left(\bigcup_{l=0}^h \theta_{f_l}\right) \cup \theta_g$ and the architecture is illustrated in Figure 6. The algorithmic procedure is identical to the DQN outlined in Mnih et al. (2015), and the approach is compatible with further modifications like Schaul et al. (2015), Van Hasselt et al. (2016), or Waltz and Okhrin (2022).

3.3. Observation and action spaces

We define $o_{OS,t}$, the OS-related component of the observation at time t, by considering the OS's velocity information, rudder angle, together with the Euclidean distance $d_{OS,t}^{G}$ and relative bearing $\alpha_{OS,t}^{G}$ to the goal $(x_{n,G}, y_{n,G})$:

$$o_{OS,t} = \left(\frac{u_t}{u_{\text{scale}}}, \frac{v_t}{v_{\text{scale}}}, \frac{\tilde{r}_t}{\tilde{r}_{\text{scale}}}, \frac{\dot{\tilde{r}}_t}{\dot{\tilde{r}}_{\text{scale}}}, \frac{\delta_t}{\delta_{\text{scale}}}, \frac{d_{\text{OS},t}^{\text{G}}}{d_{\text{scale}}}, \frac{[\alpha_{\text{OS},t}^{\text{G}}]_{-\pi}^{\pi}}{\pi}\right)^{\top}.$$

The denominators are scaling factors: $u_{\text{scale}} = 7 \,\text{m/s}$, $v_{\text{scale}} = 0.7 \,\text{m/s}$, $\tilde{r}_{\text{scale}} = 0.004 \,\text{rad/s}$, $\dot{\tilde{r}}_{\text{scale}} = 8 \cdot 10^{-5} \,\text{rad/s}^2$, $\delta_{\text{scale}} = 20 \,\text{NM}$ to achieve inputs approximately in the interval [-1,1]. To define $o_{TS,t}$, the feature vector about the target ships at time t, we assume access to AIS data of opposing ships to receive their course, speed, and positional information, which serve as input to our Deep Q-Network. Precisely, the component is defined as:

$$o_{TS,t} = (o_{1,t}, \dots, o_{N_t,t})^{\top},$$

where $o_{i,t}$ with $i=1,\ldots,N_t$ is the information about the *i*th target ship at time t, which are sorted with respect to ascending collision risk, following the newly defined metric in Section 2.3.2. To stress again: The size of $o_{TS,t}$ depends on N_t . The feature vector for TS i is defined as:

$$o_{i,t} = \left(\frac{[C_{T,i,t}]_{-\pi}^{\pi}}{\pi}, \frac{U_{i,t}}{u_{\text{scale}}}, \frac{d_{\text{OS},t}^{i} - D(\alpha_{\text{OS},t}^{i})}{d_{\text{scale}}}, \frac{[\alpha_{OS,t}^{i}]_{-\pi}^{\pi}}{\pi}, \sigma_{i,t}, CR_{i,t}\right)^{\top}$$

where $\sigma_{i,t}$ is the COLREG-encounter situation from Table 1. The element $CR_{i,t}$ is our collision risk metric for ship i at time t. Crucially, if no target ship is present, our recurrent structure still requires information about at least one ship. In this case, we artificially create a no-risk target ship $o_{TS,t} = o_{1,t} = (-1,0,1,-1,0,0)^{\top}$. This technical padding procedure is unavoidable when dealing with neural networks. However, due to our recursive structure, we need to pad information about one ship maximally instead of padding the whole surrounding area, as is the case when specifying a non-recursive architecture.

Regarding the action space, the agent can only control changes in the rudder angle by selecting one of three actions: $a_t \in \{0, -\Delta\delta, \Delta\delta\}$. We set $\Delta\delta = 5^{\circ}$ in our simulation, which builds together with our simulation step size of three seconds a realistic steering behavior of $\approx 1.67^{\circ}/s$. Further, we clip the rudder angle to an absolute value of 20°. We do not allow for thrust control to keep the action space as simple as possible, and, in practice, steering is generally preferred over thrust changes, especially for a large tanker like the KVLCC2. Thus, we keep the revolutions per second of the propeller fixed to 1.8 for the OS, which results in a speed of $\approx 7.42 \,\mathrm{m/s}$ without steering.

3.4. Reward design

We try to keep the reward function as simple as possible, but we still identified five necessary components to build an end-to-end agent that receives positional and motion information and controls the rudder angle. We must admit that many parameters are experimentally obtained in order to obtain the best performance. Building on Xu et al. (2022a), the first two components are a heading and distance reward, which enable the agent to construct a path towards the goal:

$$r_{\text{dist},t} = \frac{d_{\text{OS},t-1}^{\text{G}} - d_{\text{OS},t}^{\text{G}}}{c_7} + c_8, \qquad r_{\text{head},t} = -\frac{|[\alpha_{\text{OS},t}^{\text{G}}]_{-\pi}^{\pi}|}{\pi},$$

with constants $c_7 = 20$, $c_8 = -1$. These values result in a maximum distance reward of approximately 0 per time step, while the heading reward is in [-1, 1]. Such normalizations are helpful for interpreting the final performance of the agent. The third reward constituent penalizes collision risk by considering all other vessels via $r_{\text{coll},t} = \sum_{i=1}^{N_t} r_{\text{coll},i,t}$, where the component for TS i is:

$$r_{\text{coll},i,t} = \begin{cases} c_9 & \text{if } CR_{i,t} = 1, \\ -\sqrt{CR_{i,t}} & \text{otherwise,} \end{cases}$$

where $c_9 = -10$. Using the square root in the reward calculation deviates from prior linear suggestions, e.g., Chun et al. (2021). We found this adjustment useful because, since $CR_{i,t} \in [0,1]$, it penalizes the risk of a collision earlier and incentives the agent to develop a more foresighted behavior. Further, we include a large negative penalty in case of a collision.

The fourth component is responsible for COLREG compliance since it penalizes the agent if it does not turn right in head-on and starboard crossing situations for vessels where the CPA has not been passed yet. We set: $r_{\text{COLREG},t} = \sum_{i=1}^{N_t} r_{\text{COLREG},i,t}$, with the component for TS i being:

$$r_{\text{COLREG},i,t} = \begin{cases} c_{10} & \text{if TCPA}_{i,t} \ge 0 \text{ and } \tilde{r}_t < 0 \text{ and } \sigma_{i,t} \in \{1,2\}, \\ 0 & \text{otherwise,} \end{cases}$$

for the constant $c_{10} = -1$. We chose the yaw rate as a criterion instead of the rudder angle (as in Xu et al. 2020) since the yaw rate is, by definition, the change in heading and quantifies the actual turning of the ship's nose. In the

ship dynamics, there can be a delay of several time steps in the translation from a sign change in rudder angle to a sign change in yaw rate, making the rudder angle less adequate to judge whether a ship turns correctly.

The final reward quantity is an adaptive comfort reward that penalizes steering if there is no or only a small risk of collision. Precisely, we have:

$$r_{\text{comf},t} = \begin{cases} c_{11} & \text{if } a_t \neq 0 \text{ and } \forall i \in 1, \dots, N_t : CR_{i,t} \leq c_{12}, \\ 0 & \text{otherwise,} \end{cases}$$

where we set $c_{11} = -1$ and $c_{12} = 0.2$ in our simulation. We want to achieve a moderate and practically possible steering behavior with the comfort reward, which avoids a nonhuman succession of high-frequent course alterations. The total reward at a step t is constructed as:

$$r_t = r_{\text{dist},t} w_{\text{dist}} + r_{\text{head},t} w_{\text{head}} + r_{\text{coll},t} w_{\text{coll}} + r_{\text{COLREG},t} w_{\text{COLREG}} + r_{\text{comf},t} w_{\text{comf}},$$

for weights $w_{\rm dist} = \frac{0.05}{6.15} \approx 0.0081, w_{\rm head} = \frac{2.0}{6.15} \approx 0.3252, w_{\rm coll} = \frac{1.8}{6.15} \approx 0.2927, w_{\rm COLREG} = \frac{2.0}{6.15} \approx 0.3252,$ and $w_{\rm comf} = \frac{0.3}{6.15} \approx 0.0488$. The weights have been identified experimentally by running a grid search over different configurations.

4. Training

4.1. Environmental setup

We consider a simulation environment with $x_n, y_n \in [-7 \text{ NM}, 7 \text{ NM}]$. First, we uniformly sample an OS heading from $\{0, \frac{\pi}{2}, \pi, \frac{3}{2}\pi\}$. Afterward, the position of the OS in $\{n\}$ is set so that it is in 25 min in simulation time at $o_n = (0,0)$ if no steering takes place. The goal coordinate is initiated at the same distance but mirrored on o_n . Once OS and goal are set, to improve generalization, we randomly disturb the OS's heading by a realization of a uniform distribution $\mathcal{U}(-5^{\circ}, 5^{\circ})$. Figure 7 shows the possible constellations of the OS and the goal.

To generate the target vessels, we randomly sample a number of target ships from $\{0, 1, 2, 3\}$ with probabilities $\{0.1, 0.3, 0.3, 0.3\}$, allowing for a robust and general final agent. Afterward, we run the following COLREG-based routine for initiating a vessel:

• First, we uniformly sample a COLREG situation $\sigma \in \{0, 1, 2, 3, 4\}$ and a corresponding heading intersection angle from the intervals in Table

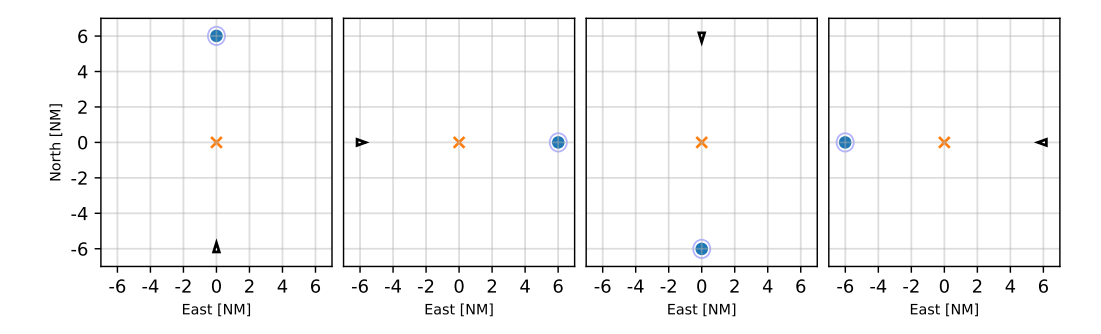


Figure 7: OS and goal spawning constellations. The black triangle is the OS, the orange cross is o_n , and the blue dot is the goal. The blue circle around the goal indicates the area (with radius $3L_{pp}$) which we consider as reaching the goal.

- 1. If $\sigma=0$, the null case, we randomly generate this angle from $\mathcal{U}(-67.5^{\circ}, 67.5^{\circ})$, which constructs a ship with a similar course as the OS. We found the inclusion of this case crucial since such cases do otherwise not appear when pursuing a COLREG-dependent spawning procedure.
- Second, we sample a propeller movement from $\mathcal{U}(0.9, 1.1) \cdot 1.8$ revolutions per second, guaranteeing the existence of slower and faster ships than the OS. Some prior work, e.g., Zhai et al. (2022), initiates all vessels at low or zero speed, which results in an acceleration phase with increased vessel maneuverability. We avoid this simplifying procedure by solving the system of equations (2) for the longitudinal speed u (fixing v = r = 0) and initiate the speed of the TS to the resulting value. The same procedure is pursued for the OS. Further, when $\sigma = 4$ (overtaking), we multiply the derived speed of the TS by a realization from $\mathcal{U}(0.3, 0.7)$, ensuring the vessel is slow enough to be overtaken.
- Third, having the angle and velocity of the TS, we determine its position in $\{n\}$ by sampling a time t_0 from $\mathcal{U}(0.75, 1.0) \cdot 25$ min. The OS's advancement in the goal direction during t_0 is computed by determining the relative velocity of the OS towards the goal and forecasting this velocity over t_0 . The procedure yields a point (x_{n,t_0}, y_{n,t_0}) . The TS is initiated to be after time t_0 at (x_{n,t_0}, y_{n,t_0}) , creating the necessity of the OS to steer and avoid a collision. This is contrary to prior work, e.g., Xu et al. (2022a), in which multiple target ships are randomly

spawned in a simulation environment while leaving the possibility of not creating a threat to the OS.

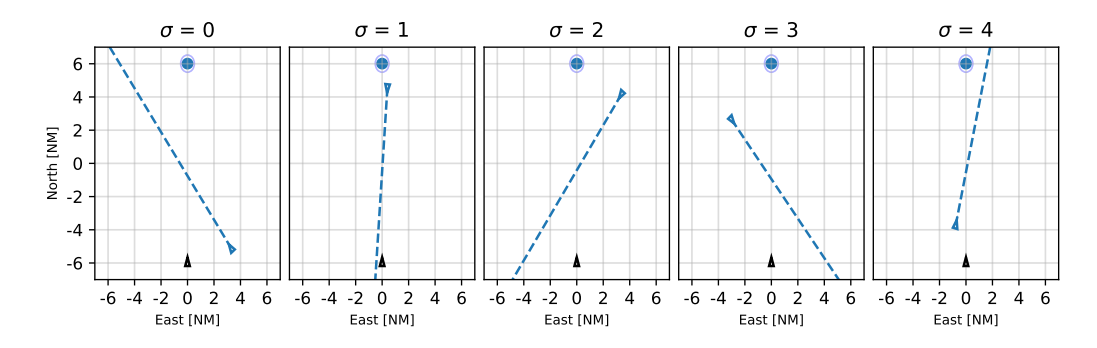


Figure 8: Sample of possible one-ship encounters during training.

Figure 8 visualizes exemplary scenarios in the case of one TS. An episode ends if the goal is reached or the number of episode steps is 1500. Crucially, we do not consider a collision an episode-ending event during training since we want to increase the number of highly negative reward transition tuples in the replay buffer. Recent research from other traffic simulations (Wurman et al., 2022) shows that focusing on high-risk scenarios improves the robustness of the converged policy.

4.2. Algorithm configuration and results

We run the algorithm of Section 3.2 for 10⁷ steps. Table 2 shows the hyperparameters, while the source code is accessible at https://github.com/MarWaltz/TUD_RL of the RL Dresden. During training, we compute every 5 000 steps the sum of rewards, called test return, of 10 evaluation episodes, average them, and exponentially smooth the results for clarity. Figure 9 displays the training performance, showing a relatively stable improvement over the considered time steps.

5. Validation

5.1. Around the Clock

We validate the trained agent in a variety of single and multiple-ship encounters. First, regarding single-ship situations, we create the 24 Around the Clock problems. These situations correspond to 24 equally spaced TS

Hyperparameter	Value				
Batch size	32				
Discount factor (γ)	0.999				
Loss function	Mean squared error				
Min. replay buffer size	1 000				
Max. replay buffer size	10^{5}				
Optimizer	Adam (Kingma and Ba, 2014)				
Target network update frequency	1 000				
Initial exploration rate $(\epsilon_{\text{initial}})$	1.0				
Final exploration rate $(\epsilon_{\text{final}})$	0.1				
Test exploration rate (ϵ_{test})	0.0				
Exploration steps	10^{6}				
Time steps	10^{7}				
History length (h)	2				

Table 2: List of hyperparameters. The ϵ of the ϵ -greedy exploration scheme, which selects a random action with probability ϵ and a greedy action otherwise, is from 1.0 linearly decayed over 10^6 steps to a final value of 0.1.

headings in the interval $(0, 2\pi)$. Precisely, we have: $\phi_{TS,j} = \frac{j}{25} \cdot 2\pi$ for $j = 1, \ldots, 24$, where j is the case number. Similar to Section 4.1, we initialize the OS and TS to be after 25 min at $o_n = (0,0)$ and place the goal on the opposite side of the simulation area. The revolutions per second are 1.8 for all vessels. Figures 10 and 11 show the trajectories and the OS's rudder angle, respectively, while the distances between the OS and the TS are depicted in Figure B.1 in Appendix B.

Analyzing the trajectories, the OS successfully reaches the goal while avoiding a collision with the linear-moving TS. The minimum encounter distance between the ships is, in all cases, larger than zero. Cases 1-6 are especially remarkable since the agent decides to pursue a turning maneuver to maintain a safe distance from the other vessel. For later situations, this turn appears unnecessary, and the agent selects COLREG-compliant right-steering to avoid, e.g., the starboard crosser in case 16. An interesting trajectory is observed in the last case, where the OS turns immediately to the starboard side to let the target vessel pass. After completing the turning maneuver, the agent moves towards the goal while the TS is already at a safe distance.

Moreover, the steering behavior of the agent is relatively moderate, although there are cases, e.g., 7 and 8, where the OS selects a sequence of

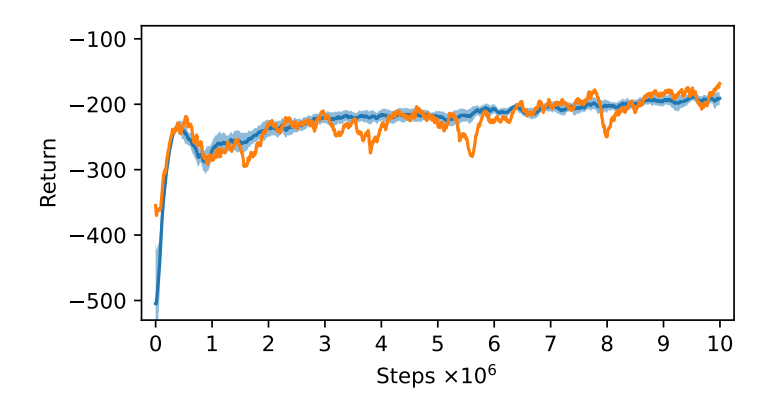


Figure 9: Test return over the training steps. The orange curve is the original run, which is used for validation. For comparison, we repeat the training and construct the blue curve as a mean over 15 independent seeds. The shaded area around the blue curve depicts 95% point-wise confidence intervals and shows the algorithm's stability.

alternating large positive and negative rudder angles. However, since one trajectory corresponds to over one hour in real-time, the angles are still real-istic. Interestingly, the agent has around half an hour of not steering in case 24, showing the ability to successfully keep a path towards the goal when no critical TS is present.

5.2. Imazu problems

The second set of validation scenarios are the Imazu problems (Imazu, 1987; Sawada et al., 2021; Zhai et al., 2022), a collection of single- and multiship encounters. The initial constellations of the target ships are detailed in Table C.1 of Appendix C, while Figures 12, 13, and 14 show the trajectories, distances between the OS and the target ships, and the rudder angles of the agent, respectively. Similar as in the Around the Clock scenarios, the agent smoothly reaches in all problems the desired goal area while successfully avoiding collisions with target ships. Moreover, the COLREG-compliance is shown since the agent avoids head-on target ships and starboard-crossers through steering to the right; see, e.g., cases 1, 2, 19, or 22. Moreover, following rule 8 of the COLREGs, the agent takes substantial collision avoidance actions in these cases, which result in a sufficient perception of the agent's steering behavior through other ships in a situation at sea. Additionally, we do not observe any undesired bow-crossing of target ships, indicating the benefit of incorporating the factor f_{DCPA} in (6).

An interesting characteristic of the agent's steering behavior is the frequent use of turning maneuvers. In the five cases 4, 10, 11, 13, and 16, the OS performs a starboard turn, which occurs at different times throughout the respective episode depending on the distance to the relevant TS. Such an advanced turning maneuver was also observed in Sawada et al. (2021), whose agent performed a starboard turn only in case 4 of the same problem set. The authors attributed the ability to perform such a turning maneuver to the specification of a continuous action space in the RL algorithm. However, due to our spatial-temporal recurrent neural architecture, we realize an efficient information processing that still allows for such maneuver with our simple, discrete action space.

Finally, the rudder movement of Figure 14 displays the low frequency of steering actions with long phases of no steering at all; see, e.g., case 11 or 18. We see through these validation scenarios that our approach results in a robust policy which can safely handle complicated real-life situations.

5.3. Star problems

The prior training and validation scenarios have assumed a linear, deterministic motion of the target ships. Of course, this assumption is unrealistic in practice, although it is frequently applied in the literature (Sawada et al., 2021; Xu et al., 2022a). To verify whether our final policy is robust enough to handle non-linear target ship movements, we create two multi-ship encounter situations called *Star problems*, which build on Zhao and Roh (2019). The scenarios include four and eight ships, respectively, and the initial headings are spaced over $[0, 2\pi)$, see Figure 15. Admittedly, the eighth-ship scenario is artificially constructed but still an interesting validation case. Each ship is initiated to reach the origin (0,0) after 25 min if no steering takes place. The goal of each ship is to reach the opposite ship's spawning area. Crucially, each vessel follows the *same policy*, which is the one validated in Sections 5.1 and 5.2.

Figure 15 displays the resulting trajectories. Each ship initially steers to the right, safely passes the other ships, and steers left to reach its goal successfully. In the case of eight ships, the collision avoidance actions are more intense, and the vessels favor a more conservative, nearly circle-shaped path, acknowledging the riskiness of a situation with so many vessels. We emphasize that these tasks are challenging since the agent has never seen more than three target ships in training nor was ever confronted with a non-linear moving ship. The policy is robust enough to manage this situation

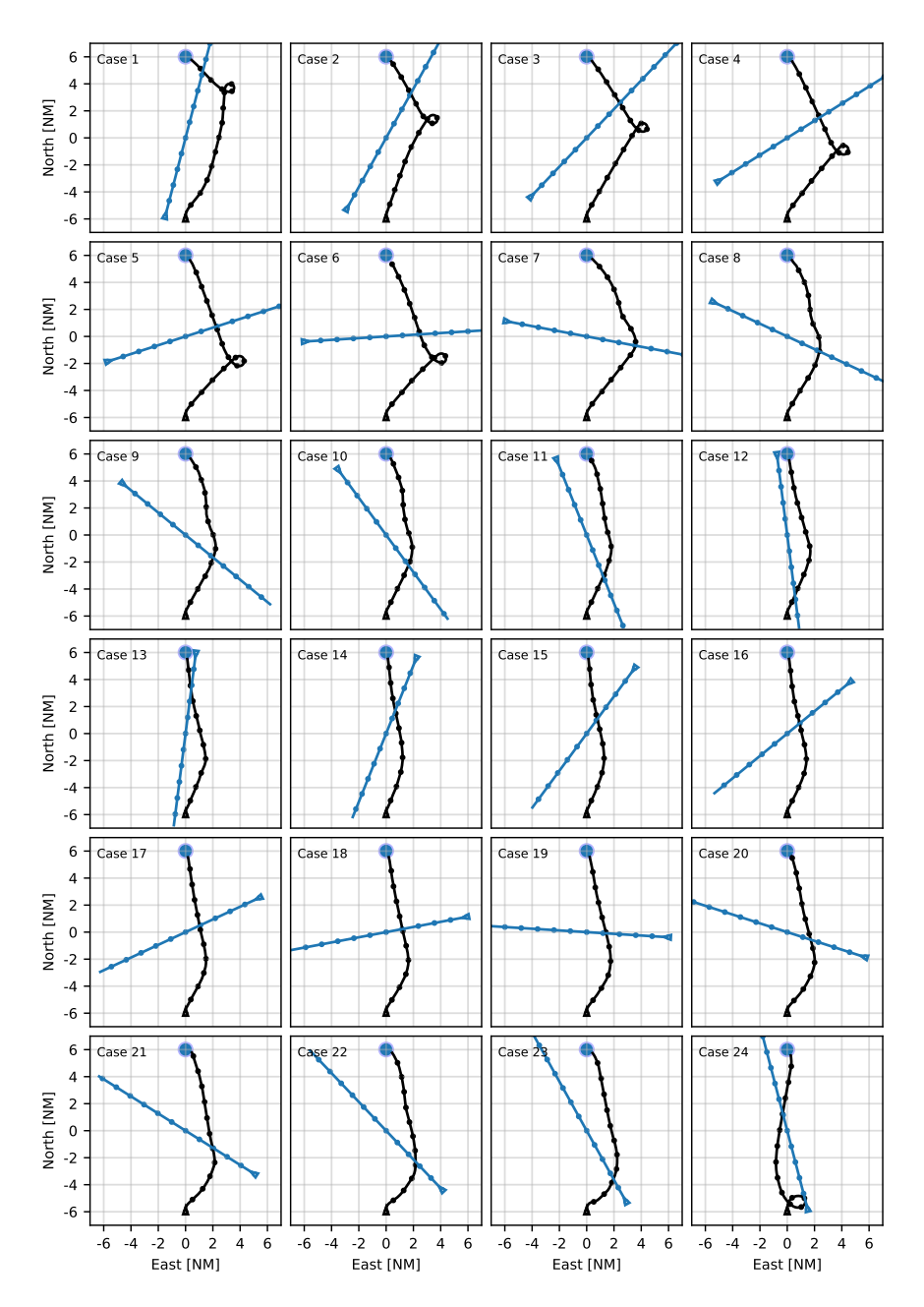


Figure 10: Around the Clock trajectories. The OS and TS trajectories are black and blue, respectively. Two consecutive dots on a trajectory correspond to a $5\,\mathrm{min}$ time interval.

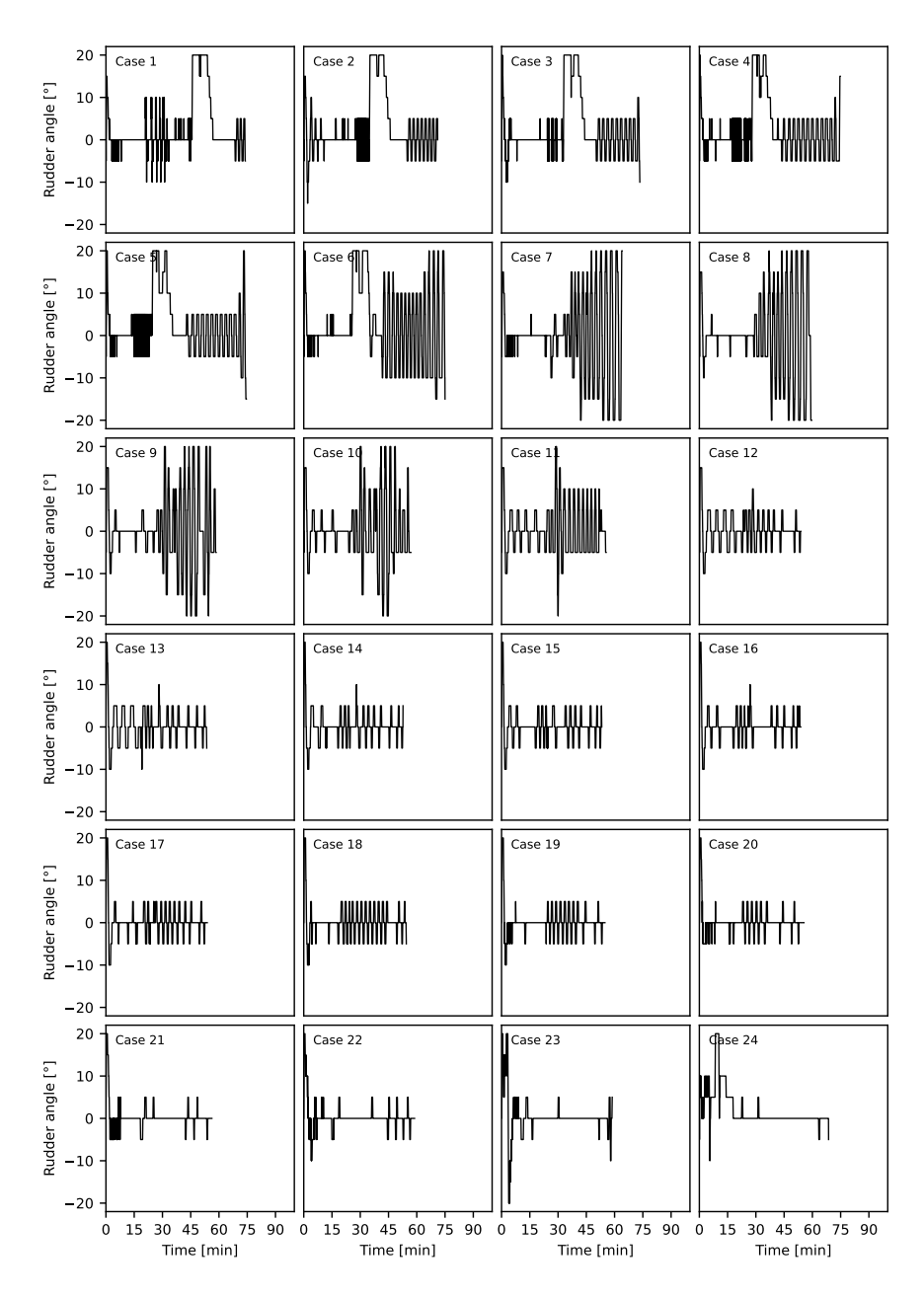


Figure 11: Rudder angles of the OS during the Around the Clock scenarios.

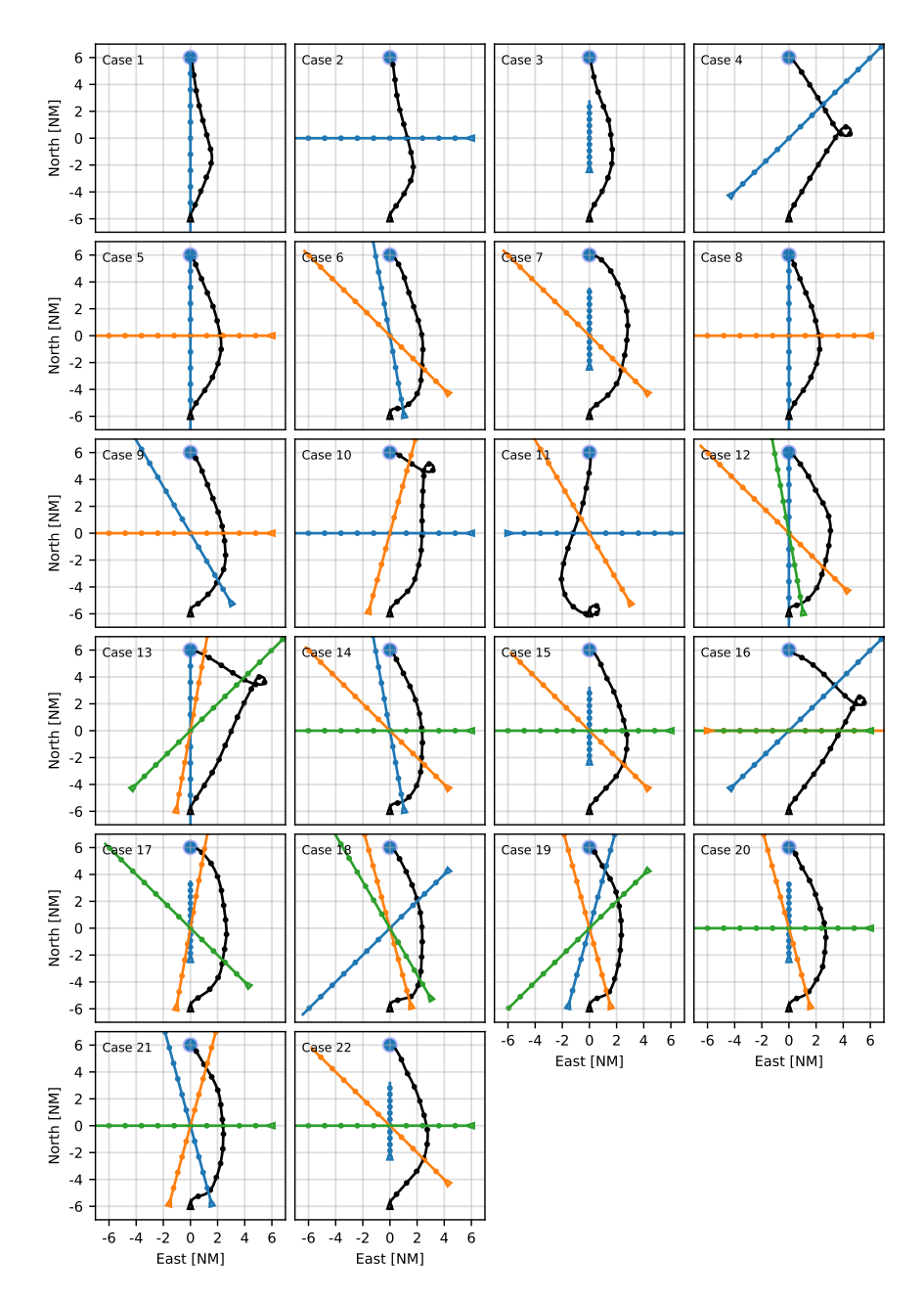


Figure 12: Trajectories on the Imazu problems. The black trajectory belongs to the own ship, while blue, orange, and green trajectories represent target ships. Two consecutive dots on a trajectory correspond to a $5\,\mathrm{min}$ time interval.

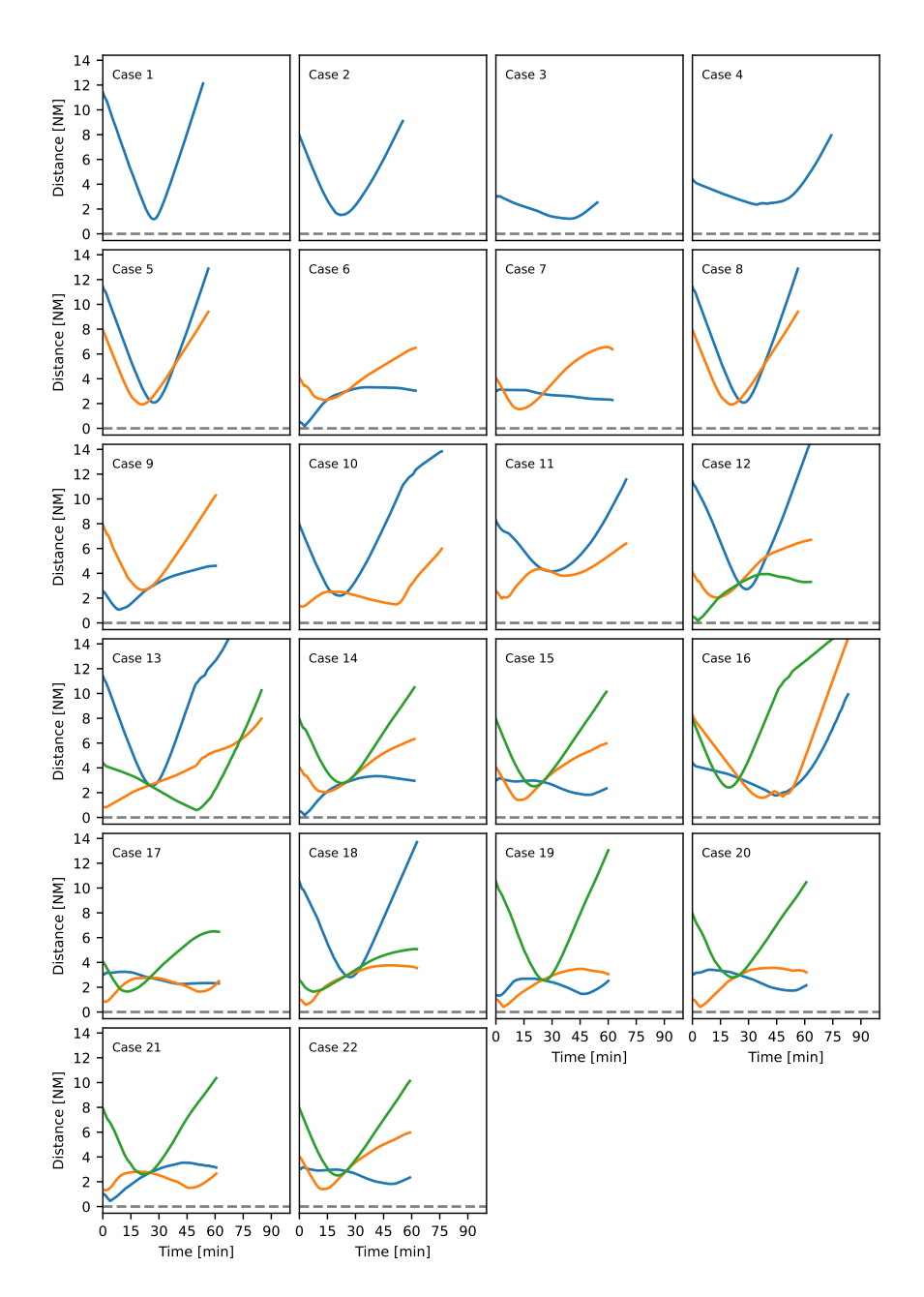


Figure 13: Distances of the own ship (agent) to the target ships on the Imazu problems. A distance of zero is not a physical collision, but means that the target ship is exactly at the border of the agent's ship domain.

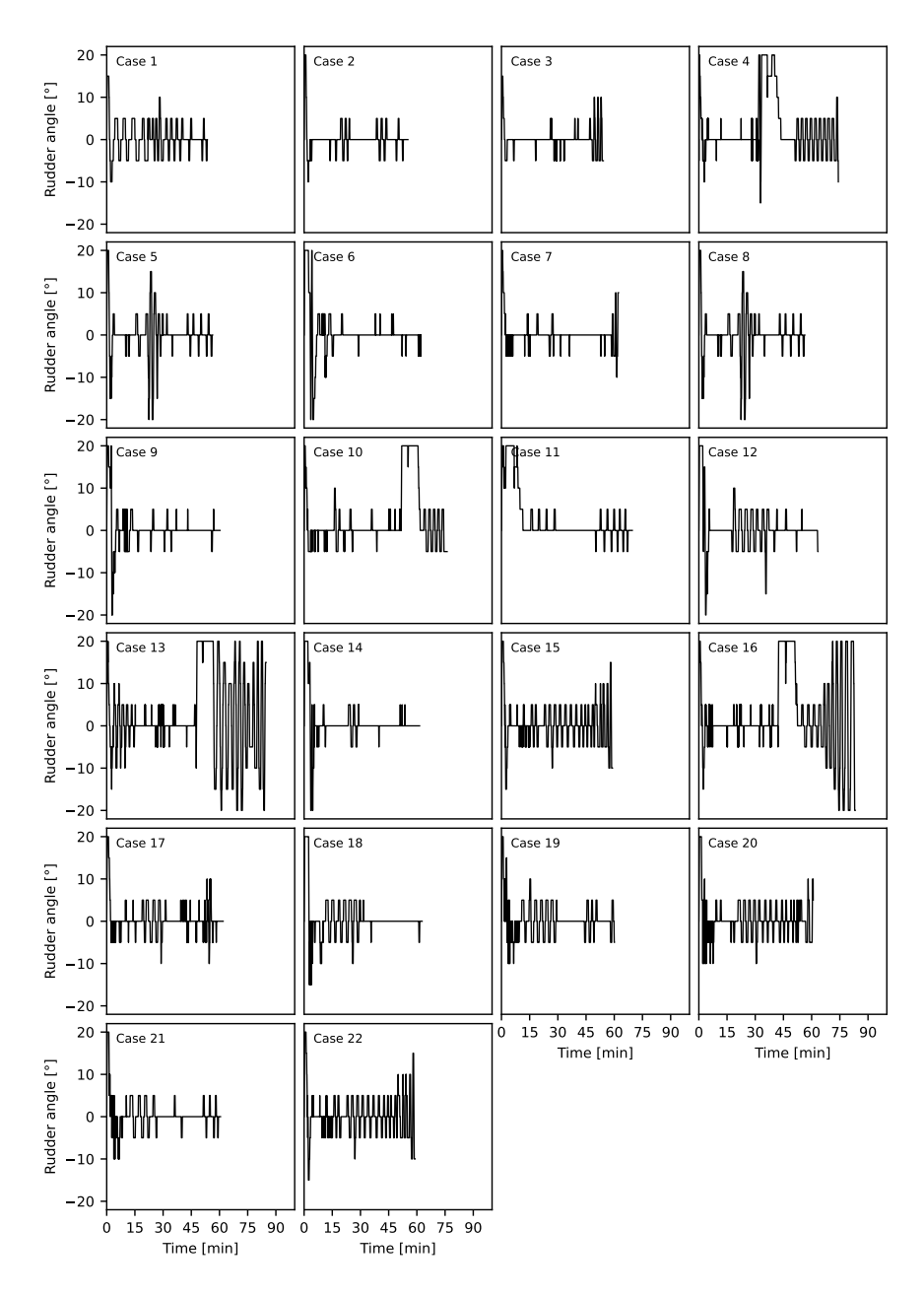
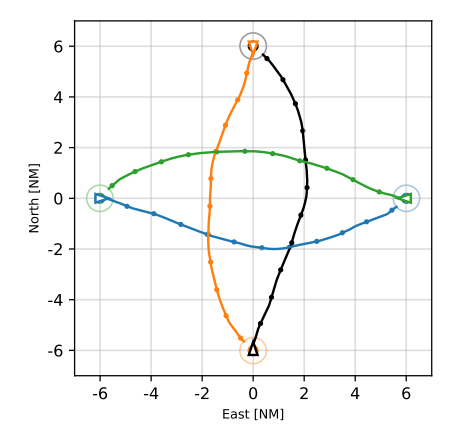


Figure 14: Steering behavior of the agent on the Imazu problems.

still. Based on these extensive validation scenarios, we showed that the neural architecture is appropriate and flexible enough to handle the complex requirements of maritime traffic.



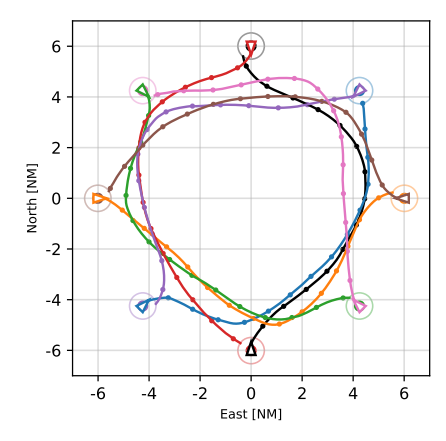


Figure 15: Validation on the Star problems. Each ship represents an RL agent and follows the same policy. Objective is to reach the opposite side.

6. Conclusion

Artificial intelligence can assist or replace human actions in critical domains to increase safety, reduce accident frequency, and save energy resources. Maritime traffic, with its traditional rule set, is such a domain in which technological advancements in the design of ASVs paired with regulatory adjustments could lead to a massive rethinking of how traffic on the sea is understood. In this paper, we designed an ASV agent using Deep Q-Networks. We embed a spatial-temporal recurrent neural network architecture in the algorithm to create a robust policy, which is validated on realistic multi-ship encounters and selects practically possible steering decisions. Equipped with a newly proposed collision risk metric, our agent can adequately assess complex situations and master advanced turning maneuvers.

We aim to address our work's limitations in future research. First, we build on the frequently imposed assumption of having no environmental disturbances in the form of wind, waves, or currents. Since those forces significantly impact real-world sea operations, we will embed them into the simulation. Second, we build on AIS data availability as an opportunity to

receive information about surrounding ships. Although our architecture is robust to partial observability, our agent is unaware of environmental characteristics such as water depth, static obstacles, or traffic participants without AIS equipment. A future fully-autonomous ASV should consider all this information by, e.g., processing LiDAR information and reading nautical maps, additionally. Finally, all of our work is done in simulation, and we plan to perform first real-world experiments with miniature vessels to validate our architecture in the field.

Acknowledgments

The authors are grateful to the Center for Information Services and High Performance Computing at TU Dresden for providing its facilities for high throughput calculations. This research did not receive any specific grant from funding agencies in the public, commercial, or not-for-profit sectors.

References

- Almalioglu, Y., Turan, M., Trigoni, N., Markham, A., 2022. Deep learning-based robust positioning for all-weather autonomous driving. Nature Machine Intelligence 4, 749–760.
- Bellemare, M.G., Candido, S., Castro, P.S., Gong, J., Machado, M.C., Moitra, S., Ponda, S.S., Wang, Z., 2020. Autonomous navigation of stratospheric balloons using reinforcement learning. Nature 588, 77–82.
- Benjamin, M.R., 2017. Autonomous COLREGS modes and velocity functions. Technical Report. Massachusetts Institute of Technology, Cambridge.
- Cheng, Y., Zhang, W., 2018. Concise deep reinforcement learning obstacle avoidance for underactuated unmanned marine vessels. Neurocomputing 272, 63–73.
- Chun, D.H., Roh, M.I., Lee, H.W., Ha, J., Yu, D., 2021. Deep reinforcement learning-based collision avoidance for an autonomous ship. Ocean Engineering 234, 109216.
- Du, Z., Negenborn, R.R., Reppa, V., 2022. COLREGS-compliant collision avoidance for physically coupled multi-vessel systems with distributed mpc. Ocean Engineering 260, 111917.

- European Maritime Safety Agency, 2021. Annual overview of marine casualties and incidents. https://www.emsa.europa.eu/newsroom/latest-news/download/6955/4266/23.html. Accessed: 2022-09-26.
- Everett, M., Chen, Y.F., How, J.P., 2018. Motion planning among dynamic, decision-making agents with deep reinforcement learning, in: 2018 IEEE/RSJ International Conference on Intelligent Robots and Systems (IROS), IEEE. pp. 3052–3059.
- Everett, M., Chen, Y.F., How, J.P., 2021. Collision avoidance in pedestrianrich environments with deep reinforcement learning. IEEE Access 9, 10357–10377.
- Fiorini, P., Shiller, Z., 1998. Motion planning in dynamic environments using velocity obstacles. The International Journal of Robotics Research 17, 760–772.
- Fossen, T.I., 2021. Handbook of Marine Craft Hydrodynamics and Motion Control, 2nd Edition. John Wiley & Sons.
- Fujimoto, S., Hoof, H., Meger, D., 2018. Addressing function approximation error in actor-critic methods, in: International Conference on Machine Learning, PMLR. pp. 1587–1596.
- Goodwin, E.M., 1975. A statistical study of ship domains. The Journal of Navigation 28, 328–344.
- Ha, J., Roh, M.I., Lee, H.W., 2021. Quantitative calculation method of the collision risk for collision avoidance in ship navigation using the cpa and ship domain. Journal of Computational Design and Engineering 8, 894–909.
- Hart, F., Okhrin, O., Treiber, M., 2022. Vessel-following model for inland waterways based on deep reinforcement learning. arXiv preprint arXiv:2207.03257.
- Hart, P.E., Nilsson, N.J., Raphael, B., 1968. A formal basis for the heuristic determination of minimum cost paths. IEEE Transactions on Systems Science and Cybernetics 4, 100–107. doi:10.1109/TSSC.1968.300136.

- Heiberg, A., Larsen, T.N., Meyer, E., Rasheed, A., San, O., Varagnolo, D., 2022. Risk-based implementation of COLREGs for autonomous surface vehicles using deep reinforcement learning. Neural Networks 152, 17–33.
- Hochreiter, S., Schmidhuber, J., 1997. Long short-term memory. Neural computation 9, 1735–1780.
- Huang, Y., Chen, L., Chen, P., Negenborn, R.R., Van Gelder, P., 2020. Ship collision avoidance methods: State-of-the-art. Safety science 121, 451–473.
- Huang, Y., Chen, L., Van Gelder, P., 2019. Generalized velocity obstacle algorithm for preventing ship collisions at sea. Ocean Engineering 173, 142–156.
- Huang, Y., Van Gelder, P., Wen, Y., 2018. Velocity obstacle algorithms for collision prevention at sea. Ocean Engineering 151, 308–321.
- Imazu, H., 1987. Research on collision avoidance manoeuvre. Ph.D. thesis. The University of Tokyo.
- International Maritime Organization, 1972. COLREG: Convention on the International Regulations for Preventing Collisions at Sea.
- Kaelbling, L.P., Littman, M.L., Cassandra, A.R., 1998. Planning and acting in partially observable stochastic domains. Artificial intelligence 101, 99– 134.
- Kang, Y.T., Chen, W.J., Zhu, D.Q., Wang, J.H., 2021. Collision avoidance path planning in multi-ship encounter situations. Journal of Marine Science and Technology 26, 1026–1037.
- Khatib, O., 1985. Real-time obstacle avoidance for manipulators and mobile robots, in: Proceedings. 1985 IEEE International Conference on Robotics and Automation, pp. 500–505. doi:10.1109/R0B0T.1985.1087247.
- Kingma, D.P., Ba, J., 2014. Adam: A method for stochastic optimization. arXiv preprint arXiv:1412.6980 .
- Kramer, O., 2017. Genetic algorithms, in: Genetic algorithm essentials. Springer, pp. 11–19.

- Lenart, A.S., 1983. Collision threat parameters for a new radar display and plot technique. The Journal of Navigation 36, 404–410.
- Li, J., Wang, H., Zhao, W., Xue, Y., 2019. Ship's trajectory planning based on improved multiobjective algorithm for collision avoidance. Journal of Advanced Transportation 2019.
- Li, L., Wu, D., Huang, Y., Yuan, Z.M., 2021. A path planning strategy unified with a COLREGS collision avoidance function based on deep reinforcement learning and artificial potential field. Applied Ocean Research 113, 102759.
- Lillicrap, T.P., Hunt, J.J., Pritzel, A., Heess, N., Erez, T., Tassa, Y., Silver, D., Wierstra, D., 2015. Continuous control with deep reinforcement learning. arXiv preprint arXiv:1509.02971.
- Liu, C., Mao, Q., Chu, X., Xie, S., 2019. An improved a-star algorithm considering water current, traffic separation and berthing for vessel path planning. Applied Sciences 9, 1057.
- Loe, Ø.A.G., 2008. Collision avoidance for unmanned surface vehicles. Ph.D. thesis. Norwegian University of Science and Technology.
- Meng, L., Gorbet, R., Kulić, D., 2021. Memory-based deep reinforcement learning for pomdps, in: 2021 IEEE/RSJ International Conference on Intelligent Robots and Systems (IROS), IEEE. pp. 5619–5626.
- Meyer, E., Robinson, H., Rasheed, A., San, O., 2020. Taming an autonomous surface vehicle for path following and collision avoidance using deep reinforcement learning. IEEE Access 8, 41466–41481.
- Miyoshi, T., Fujimoto, S., Rooks, M., Konishi, T., Suzuki, R., 2022. Rules required for operating maritime autonomous surface ships from the viewpoint of seafarers. The Journal of Navigation 75, 384–399.
- Mnih, V., Kavukcuoglu, K., Silver, D., Rusu, A.A., Veness, J., Bellemare, M.G., Graves, A., Riedmiller, M., Fidjeland, A.K., Ostrovski, G., et al., 2015. Human-level control through deep reinforcement learning. Nature 518, 529–533.

- Mou, J.M., Van Der Tak, C., Ligteringen, H., 2010. Study on collision avoidance in busy waterways by using ais data. Ocean Engineering 37, 483–490.
- Ozturk, U., Cicek, K., 2019. Individual collision risk assessment in ship navigation: A systematic literature review. Ocean Engineering 180, 130–143.
- Paszke, A., Gross, S., Massa, F., Lerer, A., Bradbury, J., Chanan, G., Killeen, T., Lin, Z., Gimelshein, N., Antiga, L., Desmaison, A., Köpf, A., Yang, E., DeVito, Z., Raison, M., Tejani, A., Chilamkurthy, S., Steiner, B., Fang, L., Bai, J., Chintala, S., 2019. Pytorch: An imperative style, high-performance deep learning library. Advances in Neural Information Processing Systems 32, 8026–8037.
- Puterman, M.L., 1994. Markov Decision Processes: Discrete Stochastic Dynamic Programming. John Wiley & Sons.
- Sawada, R., Sato, K., Majima, T., 2021. Automatic ship collision avoidance using deep reinforcement learning with 1stm in continuous action spaces. Journal of Marine Science and Technology 26, 509–524.
- Schaul, T., Quan, J., Antonoglou, I., Silver, D., 2015. Prioritized experience replay. arXiv preprint arXiv:1511.05952.
- Silver, D., Singh, S., Precup, D., Sutton, R.S., 2021. Reward is enough. Artificial Intelligence 299, 103535.
- Singh, Y., Sharma, S., Sutton, R., Hatton, D., Khan, A., 2018. A constrained a* approach towards optimal path planning for an unmanned surface vehicle in a maritime environment containing dynamic obstacles and ocean currents. Ocean Engineering 169, 187–201.
- Skjetne, R., Smogeli, Ø.N., Fossen, T.I., 2004. A nonlinear ship manoeuvering model: Identification and adaptive control with experiments for a model ship. Modeling, Identification and Control 25, 3.
- Śmierzchalski, R., 2005. Ships' domains as collision risk at sea in the evolutionary method of trajectory planning, in: Information Processing and Security Systems. Springer, pp. 411–422.

- Stern, F., Agdraup, K., Kim, S., Hochbaum, A., Rhee, K., Quadvlieg, F., Perdon, P., Hino, T., Broglia, R., Gorski, J., 2011. Experience from simman 2008—the first workshop on verification and validation of ship maneuvering simulation methods. Journal of Ship Research 55, 135–147.
- Sutton, R.S., Barto, A.G., 2018. Reinforcement Learning: An Introduction. Cambridge: The MIT Press.
- Szlapczynski, R., Szlapczynska, J., 2017. Review of ship safety domains: Models and applications. Ocean Engineering 145, 277–289.
- Treiber, M., Kanagaraj, V., 2015. Comparing numerical integration schemes for time-continuous car-following models. Physica A: Statistical Mechanics and its Applications 419, 183–195.
- Tsitsiklis, J.N., 1994. Asynchronous stochastic approximation and q-learning. Machine learning 16, 185–202.
- Vagale, A., Bye, R.T., Oucheikh, R., Osen, O.L., Fossen, T.I., 2021a. Path planning and collision avoidance for autonomous surface vehicles ii: a comparative study of algorithms. Journal of Marine Science and Technology 26, 1307–1323. URL: https://doi.org/10.1007/s00773-020-00790-x, doi:10.1007/s00773-020-00790-x.
- Vagale, A., Oucheikh, R., Bye, R.T., Osen, O.L., Fossen, T.I., 2021b. Path planning and collision avoidance for autonomous surface vehicles i: a review. Journal of Marine Science and Technology 26, 1292–1306.
- Van Hasselt, H., Guez, A., Silver, D., 2016. Deep reinforcement learning with double q-learning, in: AAAI Conference on Artificial Intelligence.
- Vinyals, O., Babuschkin, I., Czarnecki, W.M., Mathieu, M., Dudzik, A., Chung, J., Choi, D.H., Powell, R., Ewalds, T., Georgiev, P., et al., 2019. Grandmaster level in starcraft ii using multi-agent reinforcement learning. Nature 575, 350–354.
- Waltz, M., Okhrin, O., 2022. Two-sample testing in reinforcement learning. arXiv preprint arXiv:2201.08078.
- Watkins, C.J., Dayan, P., 1992. Q-learning. Machine Learning 8, 279–292.

- Woo, J., Kim, N., 2020. Collision avoidance for an unmanned surface vehicle using deep reinforcement learning. Ocean Engineering 199, 107001.
- Wu, P., Xie, S., Liu, H., Li, M., Li, H., Peng, Y., Li, X., Luo, J., 2017. Autonomous obstacle avoidance of an unmanned surface vehicle based on cooperative manoeuvring. Industrial Robot: An International Journal 44, 64–74.
- Wurman, P.R., Barrett, S., Kawamoto, K., MacGlashan, J., Subramanian, K., Walsh, T.J., Capobianco, R., Devlic, A., Eckert, F., Fuchs, F., et al., 2022. Outracing champion gran turismo drivers with deep reinforcement learning. Nature 602, 223–228.
- Xu, X., Cai, P., Ahmed, Z., Yellapu, V.S., Zhang, W., 2022a. Path planning and dynamic collision avoidance algorithm under COLREGs via deep reinforcement learning. Neurocomputing 468, 181–197.
- Xu, X., Lu, Y., Liu, G., Cai, P., Zhang, W., 2022b. COLREGs-abiding hybrid collision avoidance algorithm based on deep reinforcement learning for usvs. Ocean Engineering 247, 110749.
- Xu, X., Lu, Y., Liu, X., Zhang, W., 2020. Intelligent collision avoidance algorithms for usvs via deep reinforcement learning under COLREGs. Ocean Engineering 217, 107704.
- Yasukawa, H., Yoshimura, Y., 2015. Introduction of mmg standard method for ship maneuvering predictions. Journal of Marine Science and Technology 20, 37–52.
- Zhai, P., Zhang, Y., Shaobo, W., 2022. Intelligent ship collision avoidance algorithm based on ddqn with prioritized experience replay under COL-REGs. Journal of Marine Science and Engineering 10, 585.
- Zhao, L., Roh, M.I., 2019. COLREGs-compliant multiship collision avoidance based on deep reinforcement learning. Ocean Engineering 191, 106436.
- Zhou, C., Wang, Y., Wang, L., He, H., 2022. Obstacle avoidance strategy for an autonomous surface vessel based on modified deep deterministic policy gradient. Ocean Engineering 243, 110166.

Zhou, X.Y., Huang, J.J., Wang, F.W., Wu, Z.L., Liu, Z.J., 2020. A study of the application barriers to the use of autonomous ships posed by the good seamanship requirement of COLREGs. The Journal of Navigation 73, 710–725.

Appendix A. Selected COLREG rules

In the following, we present some of the rules from the International Maritime Organization (1972).

Rule 6: Safe speed

Every vessel shall at all times proceed at a safe speed so that she can take proper and effective action to avoid collision and be stopped within a distance appropriate to the prevailing circumstances and conditions.

Rule 7: Risk of collision

(a) Every vessel shall use all available means appropriate to the prevailing circumstances and conditions to determine if risk of collision exists. If there is any doubt such risk shall be deemed to exist.

Rule 8: Action to avoid collision

- (a) Any action to avoid collision shall be taken in accordance with the Rules of this Part and shall, if the circumstances of the case admit, be positive, made in ample time and with due regard to the observance of good seamanship.
- (b) Any alteration of course and/or speed to avoid collision shall, if the circumstances of the case admit, be large enough to be readily apparent to another vessel observing visually or by radar; a succession of small alterations of course and/or speed should be avoided.
- (c) If there is sufficient sea-room, alteration of course alone may be the most effective action to avoid a close-quarters situation provided that it is made in good time, is substantial and does not result in another close-quarters situation.
- (d) Action taken to avoid collision with another vessel shall be such as to result in passing at a safe distance. The effectiveness of the action shall be carefully checked until the other vessel is finally past and clear.

Rule 14: Head-on situation

(a) When two power-driven vessels are meeting on reciprocal or nearly reciprocal courses so as to involve risk of collision each shall alter her course

to starboard so that each shall pass on the port side of the other.

Rule 15: Crossing situation

When two power-driven vessels are crossing so as to involve risk of collision, the vessel which has the other on her own starboard side shall keep out of the way and shall, if the circumstances of the case admit, avoid crossing ahead of the other vessel.

Rule 16: Action by give-way vessel

Every vessel which is directed to keep out of the way of another vessel shall, so far as possible, take early and substantial action to keep well clear.

Appendix B. Around the Clock: Distances

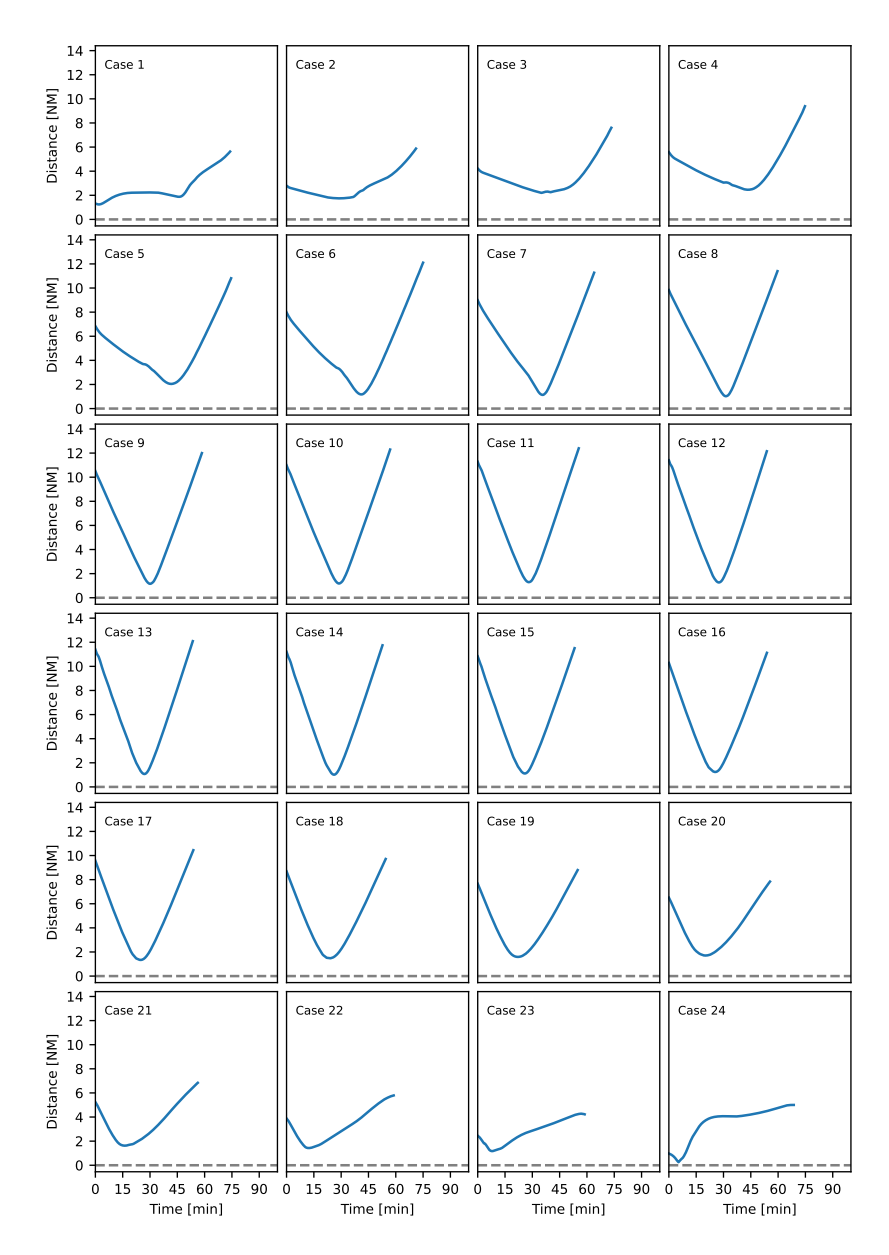


Figure B.1: Distances between OS and TS during the Around the Clock scenarios. Following our definition of a collision, a distance of zero would not equate to a physical collision, but means that the TS's midship position is exactly at the border of the agent's ship domain.

Appendix C. Imazu problem constellations

Case		Target Shi	ip 1	Target Ship 2			Target Ship 3		
	φ [°]	N [NM]	E [NM]	ϕ [°]	N [NM]	E [NM]	ϕ [°]	N [NM]	E [NM]
1	180	6.009	0.000	-	-	_	-	-	-
2	-90	0.000	6.009	-	-	-	-	-	-
3	0	-2.337	0.000	-	-	-	-	-	-
4	45	-4.249	-4.249	-	-	-	-	-	-
5	180	6.009	0.000	-90	0.000	6.009	-	-	
6	-10	-5.918	1.043	-45	-4.249	4.249	-	-	-
7	0	-2.337	0.000	-45	-4.249	4.249	-	-	-
8	180	6.009	0.000	-90	0.000	6.009	-	-	-
9	-30	-5.204	3.004	-90	0.000	6.009	-	-	-
10	-90	0.000	6.009	15	-5.804	-1.555	-	-	-
11	90	0.000	-6.009	-30	-5.204	3.004	-	-	-
12	180	6.009	0.000	-45	-4.249	4.249	-10	-5.918	1.043
13	180	6.009	0.000	10	-5.918	-1.043	45	-4.249	-4.249
14	-10	-5.918	1.043	-45	-4.249	4.249	-90	0.000	6.009
15	0	-2.337	0.000	-45	-4.249	4.249	-90	0.000	6.009
16	45	-4.249	-4.249	90	0.000	-6.009	-90	0.000	6.009
17	0	-2.337	0.000	10	-5.918	-1.043	-45	-4.249	4.249
18	-135	4.249	4.249	-15	-5.804	1.555	-30	-5.204	3.004
19	15	-5.804	-1.555	-15	-5.804	1.555	-135	4.249	4.249
20	0	-2.337	0.000	-15	-5.804	1.555	-90	0.000	6.009
21	-15	-5.804	1.555	15	-5.804	-1.555	-90	0.000	6.009
22	0	-2.337	0.000	-45	-4.249	4.249	-90	0.000	6.009

Table C.1: Starting positions of the target ships in the Imazu problems with heading angles building on Sawada et al. (2021). Note that cases 5 and 8 are identical as in Sawada et al. (2021) and Zhai et al. (2022).